energy&fuels

pubs.acs.org/EF

Article

Reducing NO_x Emission of Swirl-Stabilized Ammonia/Methane Tubular Flames through a Fuel-Oxidizer Mixing Strategy

Yuanping Yang, Qian Huang, Jinguo Sun, Peng Ma, and Shuiqing Li*

Cite This: *Energy Fuels* 2022, 36, 2277−2287

Read Online

ACCESS | Metrics & More | Article Recommendations

ABSTRACT: Ammonia as a fuel can be a carbon-free and long-duration scalable hydrogen energy carrier. In the carbon-neutral power system, co-firing ammonia with natural gas is a promising technique for flexible operations of gas turbines and gas-fired boilers. However, the NO_x propensity of ammonia/methane flames is a severe problem under global fuel-lean conditions. This work has investigated the NO_x performance of various fuel-oxidizer mixing strategies on a tangential swirl burner. We propose a new ammonia co-combustion technology with a central ammonia jet surrounded by a group of separately tangential swirl methane jets. The NO_x emissions can be reduced to about 1000 ppm under lean combustion conditions (global Φ = 0.5−0.9) when the ammonia blending ratio (E_{NH3}, in terms of input energy) is 20% (corresponding to the ammonia molar fraction x_{NH3} as 0.41). Regarding the NO_x emissions and ammonia slip at the tube exit, such a strategy outperforms other feed modes for a wide range of ammonia blending ratios (E_{NH3} up to 0.3 and x_{NH3} up to 0.52) and equivalence ratios (Φ ranging from 0.5 to 1.1). The variations of emitted NO_x with the total flow rate and the axial position of ammonia injection were also studied. Combining measurements of gaseous temperature, composition, and NH_2* chemiluminescence, we demonstrated the massive formation of NH_2 radicals in the central high-temperature ammonia-rich zone. A model involving the chemical reaction network was developed and validated against the experiments. It provides further evidence for the role of NH_2 radicals in reducing NO_x emission.

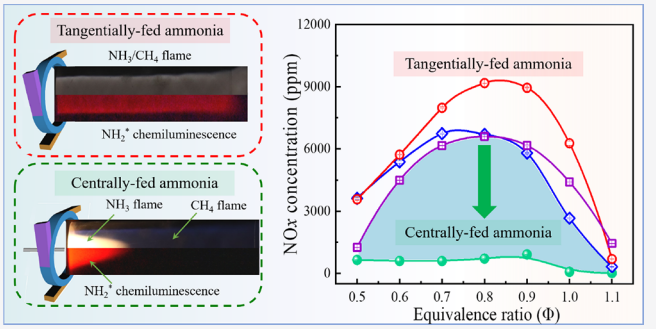

1. INTRODUCTION

The carbon-neutral power system requires high penetration of renewables generation.[1] The intermittent nature of most renewables has led to a demand for large-scale energy storage in the power system.[2] Among various storage types, chemical energy storage using synthetic fuels can accumulate energy at scales of days or even years, respond fast to load variations via combustion facilities, and enjoy the flexibility of transporting fuels.[3,4] In this way, carbon-neutral fuels serve as a replacement for fossil-fuel-based thermal power. Hydrogen is a promising energy carrier for this purpose, but its transportation, distribution, and storage are too costly and dangerous for energy use at scale.[5−7] As a feasible hydrogen carrier, ammonia (NH_3) stands out for being carbon-free, easy to liquify, and having competent H_2 density.[1,3] The mature industry of ammonia production, storage, and distribution makes it nearly ready for massive ammonia use in energy systems.[8] Though hydrogen produced by ammonia decomposition is possible, it is tempting to avoid such an energy-consuming process and utilize ammonia directly as a sustainable fuel.[1] Several technical routes have been proposed, including burning ammonia in gas turbines, fuel cells, and boilers,[9−11] and the prospect of ammonia energy has attracted global R&D investments.[12,13]

However, ammonia combustion suffers severely from flame instability and a strong propensity for nitrogen oxide (NO_x) formation. The former issue is due to the high minimum auto-ignition temperature (650 °C), the low maximum laminar burning velocity (≈7 cm/s), and the narrow flammability of ammonia.[1,14,15] A commonly-used countermeasure is to introduce other fuels as the combustor enhancer, including hydrogen,[16] carbon monoxide,[17] methane (CH_4),[18] and syngas.[19] Methane is the main component of natural gas, which is widely burnt in gas turbines and gas-fired boilers. It was reported that, with a methane blending ratio of 60% (mole fraction, E_{NH3} = 0.21) in a methane/ammonia/air flat flame, the burning velocity increases by over three times as compared with pure ammonia/air flame.[17] Moreover, the lean/rich flammability limits can be extended from Φ = 0.79−1.24 (for pure ammonia/air) to Φ = 0.61−1.40 (for ammonia with

Received: November 24, 2021
Revised: January 13, 2022
Published: January 25, 2022

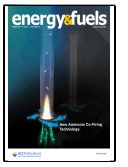

50 vol % methane blending, the corresponding E_{NH3} is 0.28).[20] On the other hand, swirl flow combustion has been widely used for flame stabilization.[21,22] In the swirl burner, fresh unburnt mixtures can be more effectively mixed and preheated by the hot, swirl-induced recirculating gas.[23,24] The recirculation zone further elongates the flow residence time.[22] It has been demonstrated that by combing these two approaches, flame stabilization is achievable for edge cases with an ammonia blending ratio as high as 80−100% of the total input energy (E_{NH3} = 0.61−1) at lab-scale combustors.[25]

While flame stability seems more tractable, the challenge of NO_x formation remains for swirl combustion of ammonia. When co-firing ammonia with methane, even if the blending ratio of ammonia is small (say, 10% of the total input energy and the ammonia molar fraction x_{NH3} is 0.22), the NO fraction in the exhaust can go up to 10^3−10^4 ppm, an unacceptable concentration higher than that from methane combustion by several orders of magnitude.[15] Some recent studies reported that premixed swirl ammonia/methane/air flames can only yield a NO concentration lower than 3000 ppm under highly fuel-rich conditions (equivalence ratio >1.1).[25,26] From a mechanistic point of view, fuel-nitrogen conversion is significantly affected by the fluid parcel history of local temperature (or heat loss), composition (important species NH_i, H, O, OH, etc.), the equivalence ratio (premixed or non-premixed and beyond or within the flammability limits), and residence time.[27−29] The optical measurement of ammonia and ammonia/hydrogen flames by combining time-resolved OH* and NH_2* chemiluminescence highlighted the important role of NH_2* in NO reduction.[30] Simultaneous OH/NO-PLIF measurements showed that the local regions of relatively high OH-PLIF intensity in the fuel-rich flame coincide with regions of relatively high NO-PLIF intensity.[15] In addition, spatial inhomogeneity stimulates more sophisticated combustion design and/or control technology. Since ammonia itself is a reductant of NO, the multi-staged combustion had been proven effective in controlling NO_x emission by constructing rich-quench-lean atmospheres in sequence.[31,32] The chemical kinetics of the air-staged combustion of ammonia/methane mixtures for reducing NO_x emission can be revealed from chemical reactor network (CRN) analysis.[33] However, the secondary air staging may result in a greater global NO_x yield through the reaction with unburnt ammonia out of fuel-rich zones.[28] Other fuel-air mixing strategies have been also explored. It is demonstrated that, for ammonia/methane mixtures, the fuel-lean non-premixed flame is less prone to NO generation than the premixed flame.[34,35] For ammonia/hydrogen mixtures, a partial premixing of H_2 coupled with non-premixed NH_3 helps reduce NO_x formation at a cost of higher ammonia slip.[30] In the ammonia/coal co-fired furnace, numerical simulation reveals that injecting ammonia into the coal-volatile-combustion region (fuel-rich zone) leads to the lowest NO_x emission.[36] These findings from different setups suggest that manipulating fuel-air injection/mixing plays an important role in the control of NO_x, but it remains unclear which strategy is the most effective.

To resolve this issue, it is noteworthy that a novel swirl-type tubular flame burner with both tangential and axial fuel inlets provides an "ideal" opportunity to evaluate different fuel-air mixing approaches.[37,38] The burner has a relatively high swirl number of around 7.0. It is designed suitable for stabilizing flames with high speed of fluid flow and for burning low-heating-value fuels such as ammonia, mainly because of the rapid mixing process and negligible heat loss behind the tubular flame.[38] As shown in our prior work,[39] fuels like methane can be fed either tangentially or axially into the burner, and both non-premixed and premixed tubular flames can be established. Hence, the various feed modes and flame structures can thus be examined to test the NO_x performance under a series of well-designed conditions, but that is rarely investigated in the literature.

This paper intensively investigated the atmospheric ammonia/methane flame that might be of significance to the development of new ammonia-fired gas boilers. In order to control NO_x formation and emission, we have schemed to investigate four kinds of flame modes of the swirl tubular flame burner, i.e., fully premixed, non-premixed (isokinetic injections with fuel dilution), non-premixed without fuel dilution, and centrally fed ammonia (with non-premixed, tangentially-fed methane, and O_2/N_2). The influences of the ammonia blending ratio (up to an input energy fraction of 0.3 and mole fraction of 0.52), equivalence ratio (from 0.5 to 1.1), and flow residence time were systematically examined. The mechanisms for NO formation and reduction were explored by combining NH_2* chemiluminescence and chemical kinetics simulations.

2. EXPERIMENTAL SECTION

2.1. Tangential Swirl Burner and Measuring System. Figure 1 shows a schematic of the experimental setup. The stainless-steel

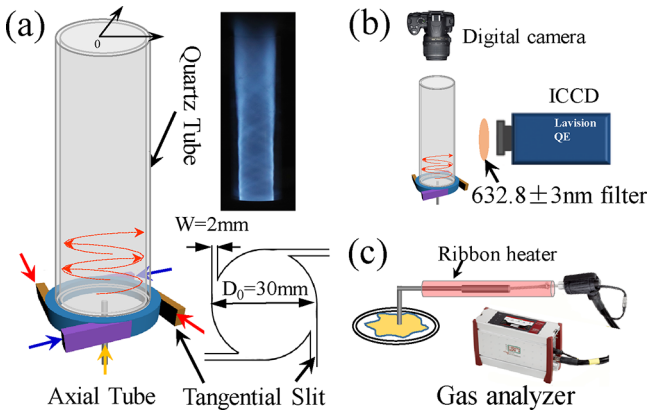

Figure 1. Schematics of (a) the tangential swirl tubular burner and a typical tubular flame, (b) optical system for flame images and NH_2* chemiluminescence, and (c) exhaust sampling and analyzing system.

burner consists of four tangential rectangular slits as reactant inlets. The width and height of the slits are 2 and 12 mm, respectively. A movable tube with an inner diameter of 2 mm is set at the center of the burner, serving as an axial inlet to achieve varied fuel-oxidizer mixing strategies. A transparent quartz tube with a 30 mm diameter and 200 mm length is applied to confine the flame (see typical tubular flame morphology in Figure 1a). More details of the burner can be seen in the literature.[40]

The tangential swirl burner has a swirl number S fully determined by the geometrical structure of the burner. The swirl number is defined as the ratio of the axial flux of angular momentum to the axial flux of linear momentum:[41]

$$S = \frac{\pi D_e D_0}{4A_T} \quad (1)$$

Here, D_0 is the diameter of the burning section (30 mm in this work), D_e is the exit throat diameter and can be approximated by subtracting the slit width W (2 mm) from the burner diameter, i.e., D_e

https://doi.org/10.1021/acs.energyfuels.1c04004
Energy Fuels 2022, 36, 2277−2287

$= D_0 - W$, and A_T is the total sectional area of the tangential inlet slits ($4 \times 2 \times 12$ mm^2). As a consequence, the calculated swirl number of the burner is about 6.87, much greater than that of the conventional swirl burner mainly with axial inlets.

The flame images were recorded by a single-lens reflex digital camera (Canon EOS Kiss X9i) through the quartz tube. The exposure times of the camera were set as 1/200 s for the top view and 1/20 s for the side view. The NH_2* chemiluminescence signal emitted from the flame can be a useful indicator of NO reduction intensity[30] and was monitored by an enhanced charge-coupled detector (ICCD, PI-Max 4) integrated with a 632.8 nm (FWHM = 3 nm) bandpass filter. The compositions of exhaust gas at the quartz tube outlet were detected by a gas analyzer (MRU-Vario Plus new), including NO, NO_2, CO, CO_2, O_2, and CH_4. A specially designed probe with an inner diameter of 1 mm was used to sample exhaust gas at more precise locations. The sampling line was heated above 120 °C to prevent water condensation and NO_2 dissolution. In addition, an ammonia analyzer based on tunable diode laser absorption spectroscopy technology (Unisearch RCP-M1-NH_3-H_2O) was utilized to evaluate the ammonia slip in different cases. For each measurement, the compositions were continuously logged for 1 min and the mean values are reported. The variance of the composition time series is usually smaller than 3% of the mean value under stabilized flame conditions. The spatial temperature distributions at different heights above the burner (HAB) were measured by a B-type thermocouple with radiation and conduction losses properly corrected.[42]

2.2. Experimental Conditions. In this work, ammonia and methane are used as the fuel, whereas the oxidizer is a mixture of oxygen and nitrogen. To clarify fueling strategic effects, Figure 2 plots

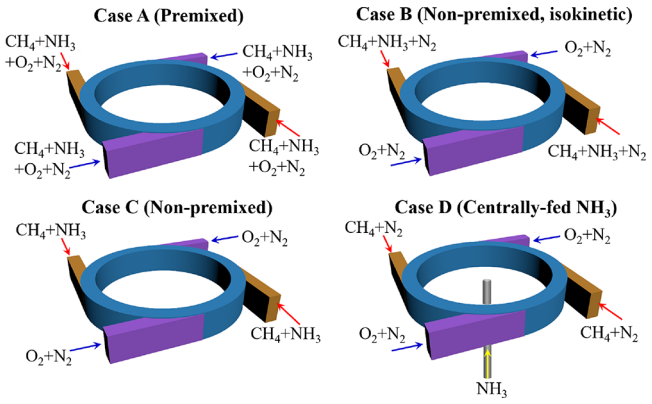

Figure 2. Four approaches for supplying fuels and oxidizer to the tangential swirl burner. Case A (premixed flame): the mixture of methane, ammonia, oxygen, and nitrogen is evenly injected into the burner through the four tangential channels; Case B (isokinetic non-premixed flame): fuels and oxidizer are fed separately from symmetric tangential slits, whereas nitrogen is added to both fuel and oxidizer as the balance gas to maintain the same injection velocity for all the inlet streams; Case C (non-premixed flame): fuel (the methane and ammonia mixture) is supplied from two non-adjacent tangential slits, and the oxidizer (oxygen/nitrogen mixture) is fed from two rest tangential slits. The total gas flow rate is kept the same as in the previous cases; Case D: ammonia is fueled through the central tube, whereas the $CH_4/O_2/N_2$ flame is burned as designed in Case B.

in detail four approaches of injecting fuels and oxidizer into the burner, and Table 1 presents the reactant flow rates under different experimental conditions at an equivalence ratio of 0.5. In the experiments, the impacts of the equivalence ratio Φ, gas flow rate, ammonia injection position, and ammonia blending ratio on NO_x emission characteristics were systematically investigated. The equivalence ratio Φ is evaluated based on the following reaction:[18]

$$n\mathrm{CH_4} + m\mathrm{NH_3} + (2n + 0.75m)(\mathrm{O_2} + 3.76\mathrm{N_2}) = n\mathrm{CO_2} + (2n + 1.5m)\mathrm{H_2O} + 3.76(2n + 0.75m)\mathrm{N_2} \quad (2)$$

Note that the combustion product of ammonia is nitrogen, rather than NO. The percentage of NH_3 in the fuel mixture is expressed in terms of the heating value as shown below:[43]

$$E_{NH_3} = \frac{x_{NH_3} \times \mathrm{LHV}_{NH_3}}{x_{NH_3} \times \mathrm{LHV}_{NH_3} + x_{CH_4} \times \mathrm{LHV}_{CH_4}} \quad (3)$$

Here, x_{NH_3} and x_{CH_4} are the mole fractions of NH_3 and CH_4 in the dual fuel mixture, and LHV denotes the lower heating value with LHV_{CH_4} = 802.30 kJ/mol and LHV_{NH_3} = 316.84 kJ/mol.

3. THEORETICAL SECTION

To better interpret the results on the tangential swirl burner, we performed chemical reaction network (CRN) analyses of nitrogen conversion in different cases using ANSYS Chemkin-PRO software version 17.2.[44] The CRN enjoys a substantial simplification of the flow field and pays more attention to the kinetic issues. A hybrid perfectly stirred reactor (PSR)−plug flow reactor (PFR) network was developed to approximate the fuel/oxidizer mixing and flue gas flow/recirculating characteristics in Cases A and D (see Figure 3a). In particular, the tangential swirl flow with strong mixing can be reasonably modeled by a PSR (denoted PSR I in Figure 3b), and the inner recirculating zone is simulated by another PSR II. Unlike a conventional axial swirl burner, our burner has a much stronger swirl flow/flame confined in the tube, so we designed a second stage of "flow-recirculation" blocks with two more PSRs III and IV that are connected in sequential with PSRs I and II (see Figure 3b). This represents the continuous mixing between the central combustion and tubular flame zones even after some distances from the burner surface and granted us more flexibility to fit the experimental results. Further downstream where the swirl is fully dissipated, the post-flame zone can be well described by a PFR with a length of 8 cm.

In Case D where ammonia is centrally fed, the CRN model introduces input ammonia into the recirculating PSR II, while in other cases, all fuels and oxidizers are fed to the PSR I. There are two splitters, denoted 1 and 2, associated with the outlets of PSRs I and III to determine the flue gas recirculating fractions. For splitter 1, the recirculating fraction was tuned in the range of 5−30%, which is consistent with the change in the ammonia blending ratio E_{NH3} varied from 0.05 to 0.3. By contrast, the recirculating fraction of splitter 2 was fixed as 10% of the flue gas flowing out of the PSR III.

In this work, the detailed mechanism for co-firing ammonia/methane was employed based on Okafor et al.[45] with over 356 elementary reactions and 59 kinds of species. Other parameters are listed in Table 2 for predicting the results in Figure 11. Briefly speaking, we tuned as few parameters as possible to fit our measured data (NO_x concentration at the tubular outlet). The residence times, estimated by the mean velocity of flue gas, were fixed for Cases A−D when only the ammonia content was changed, while it was adjusted in inverse proportion to the total gas flow rate for Case D with different gas inlet velocity.

4. RESULTS AND DISCUSSION

4.1. Characteristics of Ammonia/Methane Flames. Figure 4 presents the images of ammonia/methane flames with varied fuel/oxidizer mixing methods. It is seen from the top view that the fuels fed through the tangential slits generate

https://doi.org/10.1021/acs.energyfuels.1c04004
Energy Fuels 2022, 36, 2277−2287

Table 1. Gas Flow Rates under Various Conditions with Φ = 0.5

case	E_{NH_3}	x_{NH_3}	CH_4 (L/min)	NH_3 (L/min)	N_2 (with fuel) (L/min)	O_2 (L/min)	N_2 (with O_2) (L/min)	total gas flow rate (L/min)	thermal power (kW)
A	0.10	0.22	2.55	0.79	42.87	11.39	0	57.60	1.9
B	0.10	0.22	2.55	0.79	25.46	11.39	17.41	57.60	1.9
C	0.10	0.22	2.55	0.79	0	11.39	42.87	57.60	1.9
D	0.05	0.12	2.71	0.40	25.89	11.44	17.16	57.60	1.9
D	0.10	0.22	2.55	0.79	25.86	11.39	17.01	57.60	1.9
D	0.15	0.31	2.39	1.18	25.82	11.35	16.86	57.60	1.9
D	0.20	0.39	2.24	1.56	25.97	11.30	16.91	57.60	1.9
D	0.30	0.52	2.00	2.42	26.21	11.63	16.58	57.60	1.9
D	0.10	0.22	2.04	0.63	20.69	9.12	13.61	46.08	1.5
D	0.10	0.22	2.30	0.71	23.27	10.25	15.32	51.84	1.7
D	0.10	0.22	2.81	0.87	28.44	12.53	18.72	63.36	2.1
D	0.10	0.22	3.06	0.95	31.03	13.67	20.42	69.13	2.3

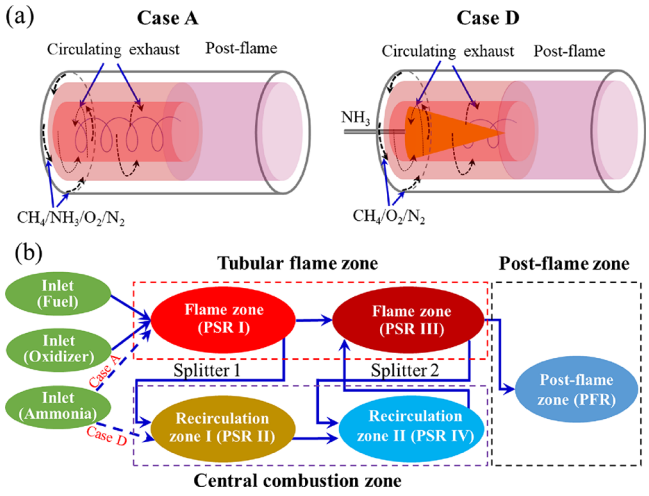

Figure 3. Reactor network representing a tangential swirl burner. (a) Schematic of fuel/oxidizer mixing and flue gas flow characteristics for Cases A and D. (b) Chemical reaction network (CRN) configuration made up by several PSRs and PFRs.

Table 2. Detailed Parameters for CRN Simulations

				residence time (s)			
case	E_{NH_3}	total gas flow rate (L/min)	split ratio 1	PSR I	PSR II	PSR III	PSR IV
A	0.10	57.60	10%	0.012	0.03	0.006	0.01
D	0.05	57.60	5%	0.012	0.03	0.006	0.01
D	0.10	57.60	10%	0.012	0.03	0.006	0.01
D	0.15	57.60	15%	0.012	0.03	0.006	0.01
D	0.20	57.60	20%	0.012	0.03	0.006	0.01
D	0.30	57.60	30%	0.012	0.03	0.006	0.01
D	0.10	46.08	10%	0.015	0.04	0.008	0.013
D	0.10	51.84	10%	0.013	0.035	0.007	0.011
D	0.10	63.36	10%	0.011	0.025	0.005	0.009
D	0.10	69.13	10%	0.009	0.02	0.004	0.008

ring-shaped, light orange flames in the thin annular area. The side-view images demonstrate that the fully premixed stream in Case A has a homogeneous flame front, and a similar structure appears in Case B with isokinetic non-premixed flame, implying the effectiveness of rapid mixing in improving the flame stability. In Case C, however, bright spiral-shaped streaks can be observed in the side view. The nonuniform flame structure is mainly ascribed to the poorer mixing of fuel and

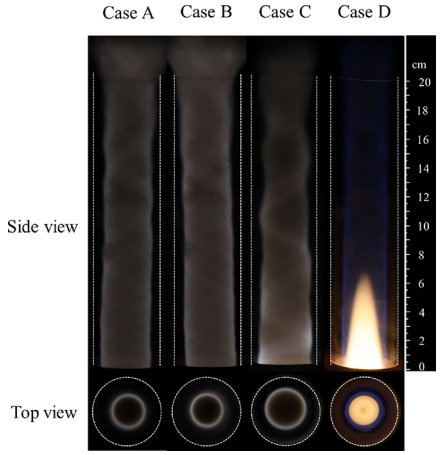

Figure 4. Instantaneous complementary metal oxide semiconductor (CMOS) photographic images of the flames in different injection strategies of ammonia with an equivalence ratio of Φ = 0.5, total flow rate of 57.6 L/min, and E_{NH_3} of 0.1 (x_{NH3} = 0.22). The dashed lines represent the outlines of the quartz tube.

the oxidizer.[46] By contrast, the centrally fed ammonia in Case D forms an orange, conical flame surface wrapped by the blue methane flame sheet (see both the top and side views). The height of the central ammonia flame is much smaller than the tube length. The visible orange chemiluminescence results from the NH_2 α-band spectra and the superheated water vapor spectra, and it becomes brighter as the equivalence ratio increases.[47] Therefore, it can be speculated from the conspicuous flame structure that the centrally fed ammonia burns under a fuel-rich condition with a much higher equivalence ratio in Case D.

We then measured the temperature and oxygen concentration at different heights above the burner (HABs) for Cases A–D, with Figure 5 showing the reconstructed smooth contours. A high-temperature annular region (above 1400 K) can be identified in Cases A, B, and C, which is consistent with the bright flame surface. Meanwhile, the central areas have relatively low temperatures (≤1310 K), and the temperatures near the tube wall even drop below 900 K in all cases due to the separation of the tubular flame from the wall. In Case D, the central ammonia flame tops 2100 K, and the reconstructed high-temperature region coincides with the visible ammonia flame exhibited in Figure 4. Similarly, the oxygen concentration is uniformly distributed (around 9 vol %) in the region with

https://doi.org/10.1021/acs.energyfuels.1c04004
Energy Fuels 2022, 36, 2277−2287

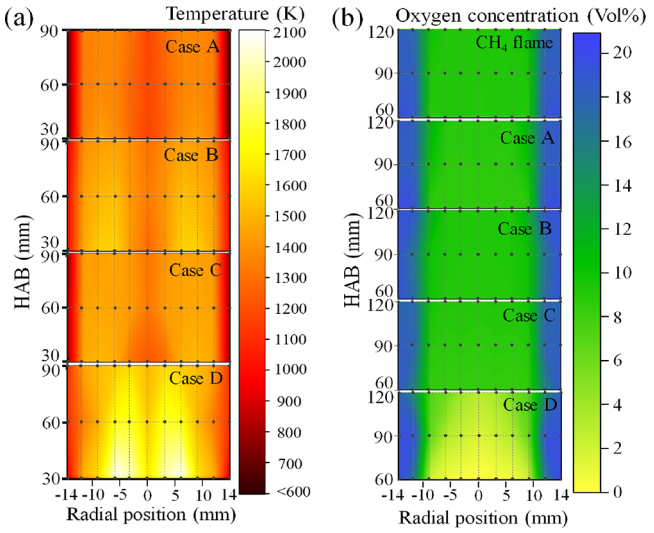

Figure 5. (a) Reconstructed temperature and (b) oxygen concentration contours of the ammonia/methane flames. The locations of the points in contours are measured and the data in the areas between points are linearly interpolated. In all ammonia co-firing cases, the equivalence ratio Φ = 0.5, total flow rate = 57.6 L/min, and E_{NH_3} = 0.1 (x_{NH3} = 0.22).

radial position $r \leq 10$ mm and the height 60 mm ≤ HAB ≤ 90 mm, as seen in Figure 5b for the pure tangentially fed methane flame and Cases A−C. Further away from the flame surface, the oxygen concentration surges to about 19 vol % in the region 12 mm ≤ r ≤ 14 mm. As for Case D, the central zone sees a depletion of oxygen with the burning of injected ammonia, especially near the ammonia outlet, clearly indicating a local fuel-rich atmosphere in such a flame configuration. Considering the nonuniform distribution of the flame in Cases B and C, we then measured the temperature distribution along the radial direction on two vertical planes in Cases B and C, and the deviations are less than 20 K for Case B and 90 K for Case C, respectively.

4.2. NO_x Emissions. *4.2.1. Effect of a Fuel-Oxidizer Mixing Strategy.* The tubular flame structure causes nonuniform distributions of exhaust gas components, as has been confirmed by oxygen in Figure 5b. We further measured the radial distributions of NO_x at the exit of the quartz tube, as presented in Figure 6a. For all cases, the NO_x concentrations at the tube exit reduce along the radial direction but significantly differ between each other. When the reactants are tangentially injected from the slits with a uniform velocity (i.e., Cases A and B), the much higher concentrations of NO_x (about 3600 ppm) at the center of the tube are produced under an equivalence ratio of 0.5. Moreover, the NO_x emissions are nearly equivalent in Cases A and B. By contrast, the production of NO_x in Case C dramatically reduces by more than 2 and 4 times, respectively, as compared with Cases A and B. Then, Case D features a vertiginous plunge of NO_x concentration with around 650 ppm at the center of the tube exit, much lower than the reported results on other types of burners in the literature.[48,49]

In addition to NO_x, Figure 6b,c presents the emitted CH_4 and CO concentrations at the tube exit to characterize the extent of burnout of the co-firing system. In Cases A and B (isokinetic fed), both CH_4 and CO are present in only trace amount (less than 0.03 vol % for CH_4 and 300 ppm for CO) within the radial position $r \leq 5$ mm, but the slips of CH_4 and

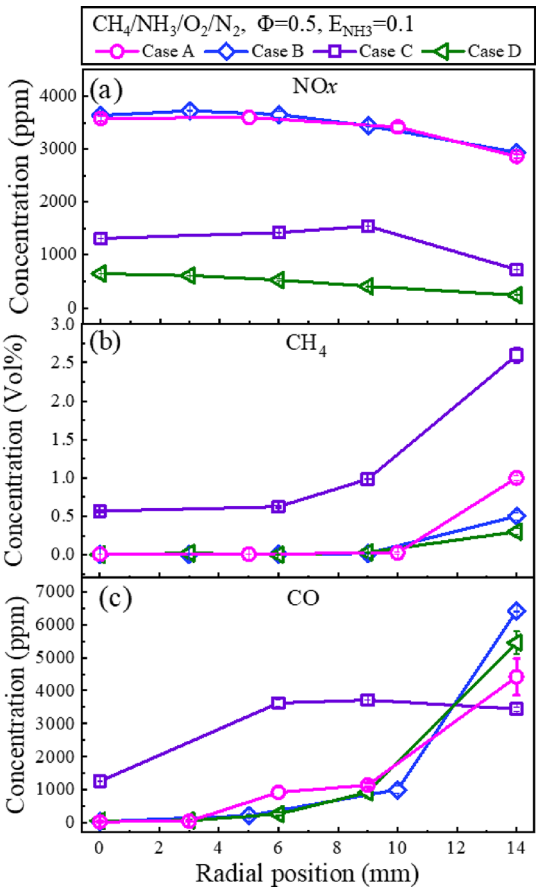

Figure 6. Radial distributions of (a) NO_x, (b) CH_4, and (c) CO concentrations at the exit of the quartz tube. For all cases, Φ = 0.5, total flow rate = 57.6 L/min, and E_{NH3} = 0.1 (x_{NH3} = 0.22).

CO become much more severely close to the low-temperature tube wall with the emitted concentrations increased by 1−2 orders of magnitude. It strongly suggests a need for designing the hot confined wall in the practical combustor. The measured ammonia slip in Cases A and B is quantified as about 1120 ppm. Nevertheless, the escaped CH_4 and CO concentrations in Case C (0.5−1.0 vol % for CH_4 and 1000−4000 ppm for CO) are significantly higher than in other cases, and the ammonia slip in Case C is more than 3000 ppm. The unburnt fuels manifest a poor mixing rate in such a non-isokinetic, non-premixed flame, indicating that it is not a suitable approach for organizing ammonia/methane/air flames, even if the measured NO_x slip is slighter. Notably, the ammonia-centrally-fed Case D has low CH_4 and CO emissions similar to Cases A and B, and in particular, the escaped ammonia is as low as only 9 ppm, which is much smaller than those of other three tangentially fed cases. Therefore, the low NO_x emissions and high burnout suggest a tantalizing prospect of ammonia axial injection in the center zone (surrounded with tangentially fed methane tubular flames) for burning nitrogen-bearing carbon-free fuels.

4.2.2. Effect of the Equivalence Ratio. Figure 7 reveals the equivalence ratio dependence (Φ = 0.5−1.1) on NO_x emissions at a fixed ammonia blending ratio E_{NH3} = 0.1 (x_{NH3} = 0.22). For all cases, the emitted NO_x concentrations are several times more than pure methane flames, increasing with the equivalence ratio in the fuel-lean regime and peak at Φ = 0.8 (or 0.9), see Figure 7a. A further increment in Φ leads

https://doi.org/10.1021/acs.energyfuels.1c04004
Energy Fuels 2022, 36, 2277−2287

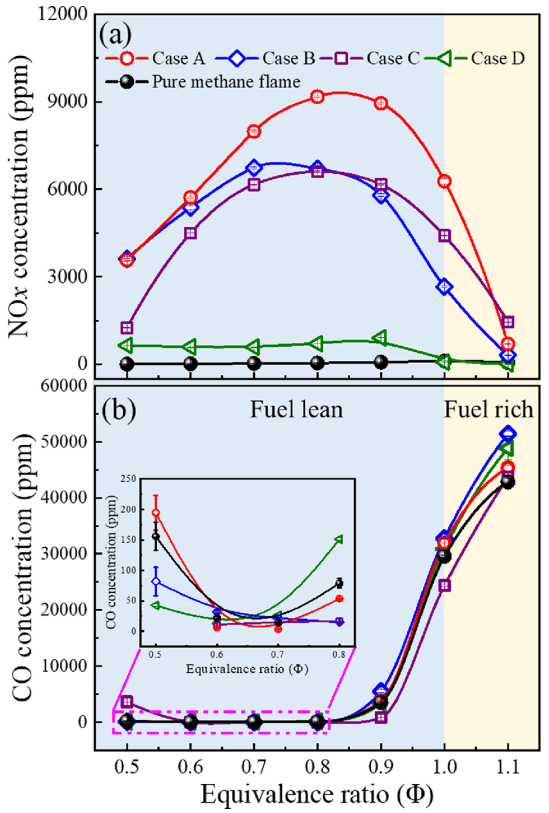

Figure 7. (a, b) Variation of emitted NO_x and CO at different equivalence ratios Φ and E_{NH_3} = 0.1 (x_{NH3} = 0.22). Note that the reported NO_x and CO concentrations are the measured values at the center of the tube exit.

to a substantial reduction of NO_x emission, which is found as 697 ppm in Case A and 319 ppm in Case B under fuel-rich Φ = 1.1, respectively. Compared with the premixed flame Case A, the non-premixed Case B enjoys remarkably lower NO_x (Figure 7a) emissions at the fuel-lean regime Φ = 0.7−1.0. It might be interpreted by the lower concentration of the OH radical in the non-premixed flame.[15] However, under fuel-lean conditions, the NO_x emissions from Cases A and B exceed 3000 ppm, posing serious challenges for the subsequent de-NO_x process. The centrally fed Case D yields much lower NO_x than other three cases for all concerned equivalence ratios. In particular, the NO_x concentration ranges 600−900 ppm for Φ < 1 and drops below 75 ppm for Φ ≥ 1. From a mechanistic point of view, the non-premixed ammonia-rich flame at the center of the tube facilitates the conversion pathway $NH_2 \rightarrow N_2$ that can avoid NO formation,[32] as evidenced by the local reducing atmosphere in Figure 5b. Moreover, the lower concentrations of O, H, and OH radicals and excess ammonia in rich flame promote NO-reducing reactions.[50] In addition to NO_x reduction, high-temperature decomposition of ammonia in the absence of oxygen is able to reinforce the flame stability.[51] We also measured the CO emission at the tubular exit in different cases, as shown in Figure 7b. It is shown that the CO emission is mainly dependent on the total equivalence ratio, and the difference among Cases A−D is marginal. In particular, for fuel-lean conditions, the CO concentration is lower than 200 ppm. As for the radial profile of CO, the significant increase for a large radius is mainly caused by the substantially lower temperatures close to the non-insulating quartz tube in our present setup (see Figure 5a). However, this is not a problem for the practical boiler in which the temperature (even near the heating surface) is much higher.

4.2.3. Effect of the Ammonia Blending Ratio. Then, we investigated the influence of the ammonia blending ratio E_{NH3} on the NO_x emissions, with the measurements of the most feasible Case D (ammonia centrally fed) presented in Figure 8. We remark that the methane flame (E_{NH3} = 0) generates NO and NO_2 concentrations less than 100 ppm. Under fuel-lean conditions, it is found that the emitted NO_x concentration increases monotonically with the blending ratio of ammonia E_{NH3}. In particular, for E_{NH3} = 0.2 (corresponding to the molar fraction x_{NH3} = 0.39), the NO_x concentration is less than 1250 ppm, far lower than those resulting from tangentially fed ammonia even with E_{NH3} = 0.1 (x_{NH3} = 0.22) (see Figure 7). For E_{NH3} = 0.3 (x_{NH3} = 0.52), NO_x concentration ranges from 1500 to 2000 ppm for Φ ≤ 0.9. Under the fuel-rich conditions (Φ = 1.0 and 1.1), the emitted NO_x concentrations decrease dramatically for E_{NH3} ≤ 0.2 because of the enhanced NO_x reduction in the presence of unburned ammonia.[52] In Figure 8b, the NO_x conversion rate is defined as the fraction of fuel-N that is converted into NO_x and is found in the range 1−5% for fuel-lean conditions.[14] Obviously, it has a similar dependence on the equivalence ratio Φ as the NO_x concentration does but seems to generally decrease as the blending ratio of ammonia E_{NH3} grows from 0.05 to 0.3. This again highlights the complex

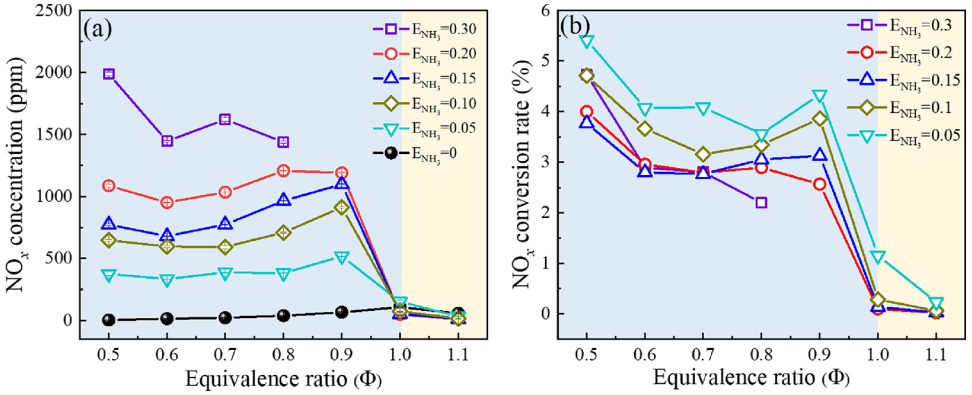

Figure 8. (a) NO_x concentration and (b) conversion rate of ammonia/methane flames as a function of the equivalence ratio for various values of E_{NH_3} (from 0.05 to 0.3, corresponding to the molar fraction x_{NH3} from 0.12 to 0.52). All the results correspond to Case D, and the total gas flow rate is kept at 57.6 L/min.

https://doi.org/10.1021/acs.energyfuels.1c04004
Energy Fuels 2022, 36, 2277−2287

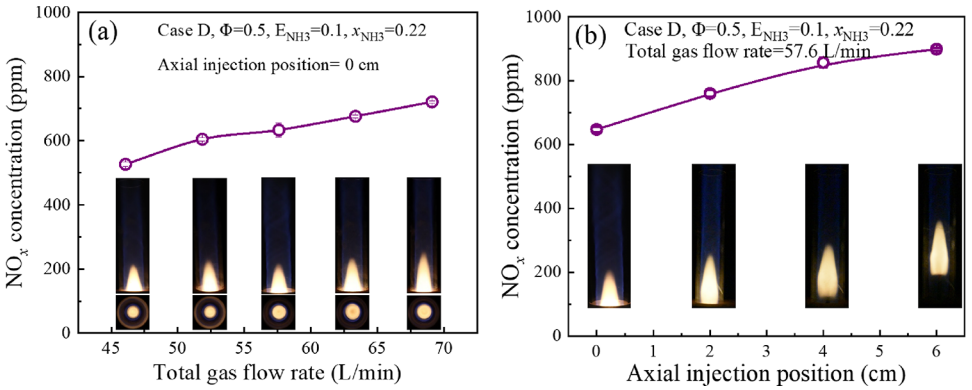

Figure 9. Effects of (a) the total injection flow rate and (b) axial injection position on NO_x emissions for Case D with $\Phi = 0.5$ and $E_{NH3} = 0.1$ ($x_{NH3} = 0.22$). Insets are the flame images under each condition.

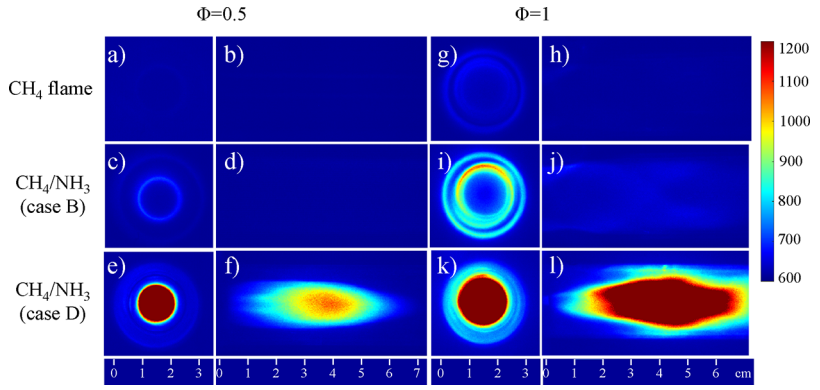

Figure 10. Time-averaged NH_2* chemiluminescence images for different ammonia fueling methods. Both top views and side views are presented. (a–f) $\Phi = 0.5$ and (g–l) $\Phi = 1$. In all cases, $E_{NH3} = 0.1$ ($x_{NH3} = 0.22$) and the total gas flow rate is kept at 57.6 L/min.

phenomena of nitrogen transformation in ammonia combustion.

4.2.4. Effect of Flow Residence Time. To further explore the performance of low-NO_x combustion with axially injected ammonia (Case D) on the tangential swirl tubular-flame burner, we manipulated the total flow residence time in the quartz tube by two methods, i.e., changing the total gas flow rate (from 46.08 to 69.13 L/min, see Table 1) and the axial height of ammonia injection (from 0 to 6 cm). Figure 9 presents the measurements of emitted NO_x for $\Phi = 0.5$ and $E_{NH3} = 0.1$ ($x_{NH3} = 0.22$). Flames are well stabilized in all the tests, as indicated by the insets of Figure 9. It is revealed that the NO_x concentration increases moderately with both the total gas flow rate (526 ppm for 46.08 L/min and 720 ppm for 69.13 L/min) and the injecting height of ammonia (633 ppm for 0 cm and 863 ppm for 6 cm). The change might be a result of the reduced residence time of ammonia and combustion products confined in the quartz tube, thus a less extent of NO reducing reactions by the unburned fuels. Some previous works reported similar influences of flow residence time on other types of combustors.[19,32,52] This calls for mechanistic explorations on nitrogen transformation in our tangential swirl burner.

4.3. Mechanistic Studies on Fuel-N Transformation.

4.3.1. NH_2 Chemiluminescence.* In this section, we measured the NH_2* chemiluminescence signal to provide direct evidence for NO consumption in ammonia flames,[30,48] and the results of different cases are shown in Figure 10. For each case, we took 100 images continuously and then averaged them to improve the signal-to-noise ratio. In the pure methane flame, the recorded signals are very weak for both equivalence ratios, which is as expected because NO is produced only in trace amount, and the signal may as well come from other broadband radiations. Thus, the weak signals from pure methane flame can be regarded as the "background" for ammonia/methane flames. In Case B (tangentially fed, isokinetic, and non-premixed flame), an annular region with strong NH_2* chemiluminescence signals is observed from the top view, which fully coincides with the flame shape illustrated in Figure 4. Also, the signal intensity for $\Phi = 1.0$ is remarkably higher than that for $\Phi = 0.5$. Considering the rather weak background in pure methane flame, we conclude that the detected signals do originate from flame-generated NH_2*, which is a key intermediate species for ammonia decomposition and NO reduction. More notably, the centrally fed ammonia in Case D leads to an inner region with very strong signals of NH_2* chemiluminescence (see Figure 10e,f,k,l), and again, this region well matches the visible ammonia flame structure. The side views of $\Phi = 0.5$ (Figure 10f) and 1.0 (Figure 10l) clearly demonstrate a negative effect of oxygen on NH_2* enrichment. The NH_2* signal seems to first increase with HAB and peaks at HAB ≈ 4 cm before starting to reduce for $\Phi = 0.5$, while for $\Phi = 1.0$, the signal becomes saturated from HAB = 2 to 6 cm. This manifests the dynamic evolution of NH_2*, which is first formed by ammonia decomposition and then gradually consumed by oxygen and NO. The possible reactions associated with NO reduction include $NO + NH_2 = NNH + OH$ and $NO + NH_2 = N_2 + H_2O$.[13,16]

4.3.2. CRN Analysis of NO Formation in Ammonia Combustion. The CRN analysis has been performed, and as

https://doi.org/10.1021/acs.energyfuels.1c04004
Energy Fuels 2022, 36, 2277−2287

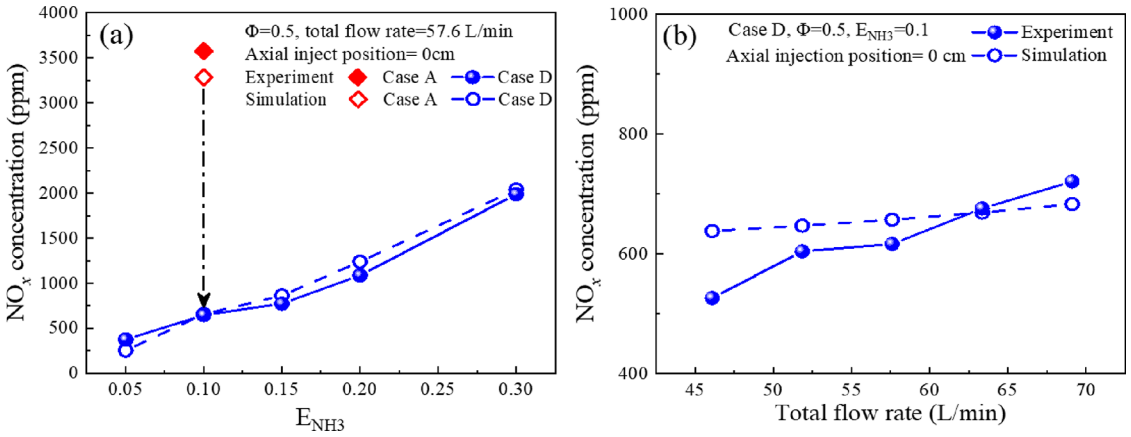

Figure 11. Comparison of emitted NO_x concentrations from measurements and CRN simulations, (a) the effects of ammonia blending ratios and (b) the effect of the total flow rate.

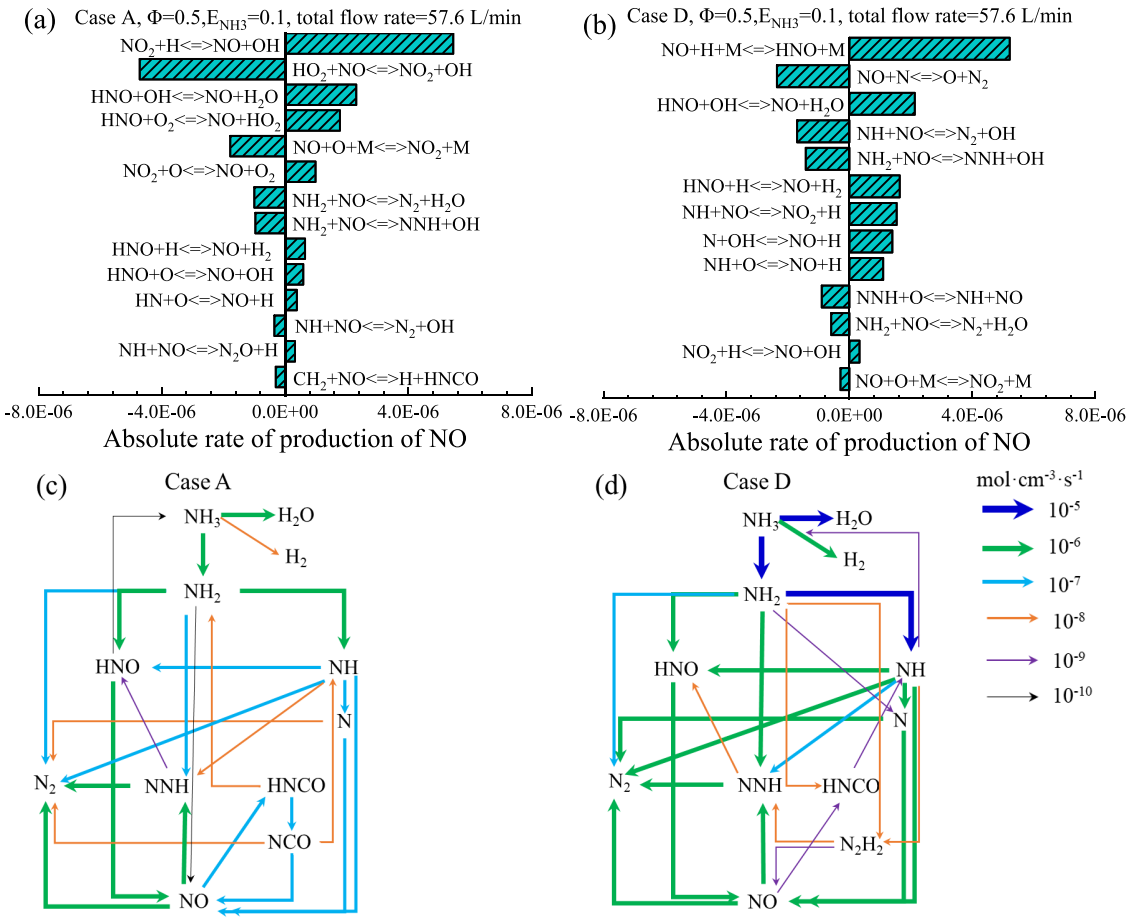

Figure 12. Absolute rates of NO production and the reaction pathways: (a, c) for PSR I of Case A (tangentially fed premixed flame) and (b, d) for PSR II of Case D (centrally fed ammonia). The width of each arrow denotes the relative magnitude of the reaction rate.

detailed in Section 3, the free parameters related to the reactors are specified in Table 2. Figure 11 shows the comparison between measured and simulated NO_x emissions for several representative cases. First, it is seen in Figure 11a that such predicted NO_x concentrations at the quartz tube outlet (HAB = 20 cm) agree reasonably with the measurements in Cases A (E_{NH3} = 0.1, x_{NH3} = 0.22) and D (E_{NH3} ranges from 0.05 to 0.3 and x_{NH3} ranges from 0.12 to 0.52). This highlights the reliability of the simplified CRN model (see Figure 3) for revealing major reaction pathways; however, we shall point out that little ammonia slip is present in the simulation, while for Case A, the measured value is 1120 ppm. The overestimated extent of mixing in the PSRs may be the main cause. Clearly, Case A (tangentially fed premixed ammonia/methane/air) is much more prone to generating NO_x than Case D (centrally fed ammonia). Figure 12 illustrates the absolute rates of NO production/destruction (a and b) and the major chemical pathways in the conversion of fuel-N (ammonia) to NO (c and d) for PSR I of Case A and PSR II of Case D. In Figure 12c,d, the width of the arrow gives

https://doi.org/10.1021/acs.energyfuels.1c04004
Energy Fuels 2022, 36, 2277−2287

a visual indication of the relative importance of a particular reaction path.

We find that in Case A, the mutual conversion of NO and NO_2, as well as the conversion of HNO, are the most important pathways of NO formation. The reduction reaction of NO by NH_2 is slower than the NO formation reactions. In Case D, NO is still mainly formed by the conversion of HNO, and the emitted NO concentration increases with E_{NH3}. Then, the reduction of NO by amine radicals (NH and NH_2) and N become more outstanding, as shown in Figure 12b. The comparison of Figure 12c,d clearly indicates that the decomposition of ammonia to NH, NH_2, and N in Case D has been significantly enhanced, which is consistent with the experimental observation of NH_2* chemiluminescence in Figure 10. Therefore, the local fuel-rich condition in Case D contributes to the much lower NO formation propensity. With an increment in the total gas flow rate (and thus a decrease in the flow residence time in the quartz tube), the emitted NO concentration increases. However, the simulated NO concentration has a smaller rate of increase with the flow rate (see Figure 11b). Again, this could be attributed to the overestimated extent of mixing in the PSRs.

5. CONCLUSIONS

This paper comprehensively investigated NO_x generation of ammonia/methane tubular swirl flames with various fuel-oxidizer mixing approaches under different operating conditions. We propose a new ammonia co-combustion technology with a central ammonia jet surrounded by a group of separately tangential swirl methane jets. This approach outperforms other investigated modes of tangentially fed ammonia (either premixed or non-premixed with O_2/N_2) in terms of both the NO_x propensity and ammonia slip. In particular, the emitted NO_x concentration is about 1000 ppm for lean combustion conditions ($\Phi = 0.5-0.9$) with the energy input rate of ammonia as 20% ($x_{NH3} = 0.39$), which is substantially lower than the reported NO_x emissions of premixed swirl ammonia/methane flames. In the fuel-lean regime, the emitted NO_x concentration increases with both E_{NH3} (at least for $E_{NH3} \leq 0.3$ and $x_{NH3} \leq 0.52$) and the equivalence ratio Φ. The NO_x concentration peaks at $\Phi = 0.8-0.9$. The reduction of flow residence time in the tube, either by delaying the injection position or elevating the total flow rate, leads to higher NO_x yields. As evidenced by the NH_2* chemiluminescence, the central high-temperature, ammonia-rich flame facilitates an extensive formation of NH_2, which is the major reductant to restrain NO_x formation. In summary, a strategy of clean and efficient ammonia co-combustion is to build an ammonia-rich zone that can rapidly mix with high-temperature, low-oxygen post-flame exhausts. Also, it is desirable for future research to further increase the ammonia blending ratio E_{NH3}.

AUTHOR INFORMATION

Corresponding Author

Shuiqing Li − *Key Laboratory for Thermal Science and Power Engineering of Ministry of Education, International Joint Laboratory on Low Carbon Clean Energy Innovation of Ministry of Education, Department of Energy and Power Engineering, Tsinghua University, Beijing 100084, China;* orcid.org/0000-0001-6278-5956; Phone: +86-010-62788506; Email: lishuiqing@tsinghua.edu.cn; Fax: +86-010-62773384

Authors

Yuanping Yang − *Key Laboratory for Thermal Science and Power Engineering of Ministry of Education, International Joint Laboratory on Low Carbon Clean Energy Innovation of Ministry of Education, Department of Energy and Power Engineering, Tsinghua University, Beijing 100084, China*

Qian Huang − *Key Laboratory for Thermal Science and Power Engineering of Ministry of Education, International Joint Laboratory on Low Carbon Clean Energy Innovation of Ministry of Education, Department of Energy and Power Engineering, Tsinghua University, Beijing 100084, China*

Jinguo Sun − *Key Laboratory for Thermal Science and Power Engineering of Ministry of Education, International Joint Laboratory on Low Carbon Clean Energy Innovation of Ministry of Education, Department of Energy and Power Engineering, Tsinghua University, Beijing 100084, China*

Peng Ma − *Key Laboratory for Thermal Science and Power Engineering of Ministry of Education, International Joint Laboratory on Low Carbon Clean Energy Innovation of Ministry of Education, Department of Energy and Power Engineering, Tsinghua University, Beijing 100084, China*

Complete contact information is available at: https://pubs.acs.org/10.1021/acs.energyfuels.1c04004

Notes

The authors declare no competing financial interest.

ACKNOWLEDGMENTS

This work was supported by the National Natural Science Foundation of China (nos. 52006121 and 51725601). We are grateful to Prof. Baolu Shi at the Beijing Institute of Technology, Prof. Chen Zheng at Peking University, Prof. Zhenyu Tian at the Institute of Engineering Thermophysics of CAS, and Dr. Minghang Song and Prof. Yun Huang at the Institute of Process Engineering of CAS for fruitful discussions.

REFERENCES

(1) Valera-Medina, A.; Xiao, H.; Owen-Jones, M.; David, W. I. F.; Bowen, P. J. Ammonia for power. *Prog. Energy Combust. Sci.* **2018**, *69*, 63−102.

(2) Carmo, M.; Stolten, D. Chapter 4 - Energy Storage Using Hydrogen Produced From Excess Renewable Electricity: Power to Hydrogen. In *Science and Engineering of Hydrogen-Based Energy Technologies*; Academic Press: 2019, 165−199, DOI: 10.1016/B978-0-12-814251-6.00004-6.

(3) Kobayashi, H.; Hayakawa, A.; Somarathne, K. D.; Kunkuma, A. Okafor, Ekenechukwu C. Science and technology of ammonia combustion. *P Combust. Inst.* **2019**, *37*, 109−133.

(4) Abe, J. O.; Popoola, A. P. I.; Ajenifuja, E.; Popoola, O. M. Hydrogen energy, economy and storage: Review and recommendation. *Int. J. Hydrogen Energy* **2019**, *44*, 15072−15086.

(5) Tarhan, C.; Çil, M. A. A study on hydrogen, the clean energy of the future: Hydrogen storage methods. *J Energy Storage.* **2021**, *40*, 102676.

(6) Huang, Y. S.; Shi, M. S.; Wang, W. Y.; Lin, H. Y. A two-stage planning and optimization model for water - hydrogen integrated energy system with isolated grid. *J. Cleaner Prod.* **2021**, *313*, 127889.

(7) Valera-Medina, A.; Marsh, R.; Runyon, J.; Pugh, D.; Beasley, P.; Hughes, T.; Bowen, P. Ammonia−methane combustion in tangential swirl burners for gas turbine power generation. *Appl Energy* **2017**, *185*, 1362−1371.

(8) Nayak-Luke, R. M.; Forbes, C.; Cesaro, Z.; Bañares-Alcántara, R.; Rouwenhorst, K. H. R. Chapter 8-Techno-Economic Aspects of Production, Storage and Distribution of Ammonia. In *Techno-*

Economic Challenges of Green Ammonia as an Energy Vector; Academic Press: 2021; DOI: 10.1016/B978-0-12-820560-0.01001-8.
(9) Honzawa, T.; Kai, R.; Okada, A.; Valera-Medina, A.; Bowen, P. J.; Kurose, R. Predictions of NO and CO emissions in ammonia/methane/air combustion by LES using a non-adiabatic flamelet generated manifold. *Energy.* **2019**, *186*, 115771.
(10) Ilbas, M.; Kumuk, O.; Karyeyen, S. Numerical study of a swirl gas turbine combustor for turbulent air and oxy-combustion of ammonia/kerosene fuels. *Fuel* **2021**, *304*, 121359.
(11) Lhuillier, C.; Brequigny, P.; Contino, F.; Mounaïm-Rousselle, C. Experimental study on ammonia/hydrogen/air combustion in spark ignition engine conditions. *Fuel* **2020**, *269*, 117448.
(12) Yapicioglu, A.; Dincer, I. A review on clean ammonia as a potential fuel for power generators. *Renew Sust Energ Rev.* **2019**, *103*, 96−108.
(13) Valera-Medina, A.; Amer-Hatem, F.; Azad, A. K.; Dedoussi, I. C.; de Joannon, M.; Fernandes, R. X.; Glarborg, P.; Hashemi, H.; He, X.; Mashruk, S.; McGowan, J.; Mounaim-Rouselle, C.; Ortiz-Prado, A.; Ortiz-Valera, A.; Rossetti, I.; Shu, B.; Yehia, M.; Xiao, H.; Costa, M. Review on Ammonia as a Potential Fuel: From Synthesis to Economics. *Energy Fuels* **2021**, *35*, 6964−7029.
(14) Kurata, O.; Iki, N.; Matsunuma, T.; Inoue, T.; Tsujimura, T.; Furutani, H.; Kobayashi, H.; Hayakawa, A. Performances and emission characteristics of NH_3−air and NH_3−CH_4−air combustion gas-turbine power generations. *P Combust. Inst.* **2017**, *36*, 3351−3359.
(15) Okafor, E. C.; Somarathne, K. D. K. A.; Ratthanan, R.; Hayakawa, A.; Kudo, T.; Kurata, O.; Iki, N.; Tsujimura, T.; Furutani, H.; Kobayashi, H. Control of NO_x and other emissions in micro gas turbine combustors fuelled with mixtures of methane and ammonia. *Combust. Flame* **2020**, *211*, 406−416.
(16) Otomo, J.; Koshi, M.; Mitsumori, T.; Iwasaki, H.; Yamada, K. Chemical kinetic modeling of ammonia oxidation with improved reaction mechanism for ammonia/air and ammonia/hydrogen/air combustion. *Int. J. Hydrogen Energy* **2018**, *43*, 3004−3014.
(17) Han, X.; Wang, Z.; Costa, M.; Sun, Z.; He, Y.; Cen, K. Experimental and kinetic modeling study of laminar burning velocities of NH_3/air, NH_3/H_2/air, NH_3/CO/air and NH_3/CH_4/air premixed flames. *Combust. Flame* **2019**, *206*, 214−226.
(18) Okafor, E. C.; Naito, Y.; Colson, S.; Ichikawa, A.; Kudo, T.; Hayakawa, A.; Kobayashi, H. Measurement and modelling of the laminar burning velocity of methane-ammonia-air flames at high pressures using a reduced reaction mechanism. *Combust. Flame* **2019**, *204*, 162−175.
(19) Ding, C.; Li, P.; Wang, K.; Shi, G.; Wang, F.; Liu, Z. Experimental and Kinetic Study on the Oxidation of Syngas-Ammonia under Both N_2 and CO_2 Atmospheres in a Jet-Stirred Reactor. *Energ Fuel.* **2021**, *35*, 11445−11456.
(20) Tang, G.; Jin, P.; Bao, Y.; Chai, W. S.; Zhou, L. Experimental investigation of premixed combustion limits of hydrogen and methane additives in ammonia. *Int J Hydrogen Energ.* **2021**, *46*, 20765−20776.
(21) Valera-Medina, A.; Pugh, D. G.; Marsh, P.; Bulat, G.; Bowen, P. Preliminary study on lean premixed combustion of ammonia-hydrogen for swirling gas turbine combustors. *Int. J. Hydrogen Energy* **2017**, *42*, 24495−24503.
(22) Reddy, V. M.; Katoch, A.; Roberts, W. L.; Kumar, S. Experimental and numerical analysis for high intensity swirl based ultra-low emission flameless combustor operating with liquid fuels. *P Combust. Inst.* **2015**, *35*, 3581−3589.
(23) Somarathne, K. D. K. A.; Okafor, C. E.; Hayakawa, A.; Kudo, T.; Kurata, O.; Iki, N.; Kobayashi, H. Emission characteristics of turbulent non-premixed ammonia/air and methane/air swirl flames through a rich-lean combustor under various wall thermal boundary conditions at high pressure. *Combust. Flame* **2019**, *210*, 247−261.
(24) Wei, X.; Zhang, M.; An, Z.; Wang, J.; Huang, Z.; Tan, H. Large eddy simulation on flame topologies and the blow-off characteristics of ammonia/air flame in a model gas turbine combustor. *Fuel* **2021**, *298*, 120846.
(25) Khateeb, A. A.; Guiberti, T. F.; Zhu, X.; Younes, M.; Jamal, A.; Roberts, W. L. Stability limits and exhaust NO performances of ammonia-methane-air swirl flames. *Exp. Therm. Fluid Sci.* **2020**, *114*, 110058.
(26) Khateeb, A. A.; Guiberti, T. F.; Wang, G.; Boyette, W. R.; Younes, M.; Jamal, A.; Roberts, W. L. Stability limits and NO emissions of premixed swirl ammonia-air flames enriched with hydrogen or methane at elevated pressures. *Int. J. Hydrogen Energy* **2021**, *46*, 11969−11981.
(27) Glarborg, P.; Miller, J. A.; Ruscic, B.; Klippenstein, S. J. Modeling nitrogen chemistry in combustion. *Prog. Energy Combust. Sci.* **2018**, *67*, 31−68.
(28) Zhu, X.; Khateeb, A. A.; Guiberti, T. F.; Roberts, W. L. NO and OH* emission characteristics of very-lean to stoichiometric ammonia−hydrogen−air swirl flames. *P Combust. Inst.* **2021**, *38*, 5155−5162.
(29) Zhu, X.; Khateeb, A. A.; Roberts, W. L.; Guiberti, T. F. Chemiluminescence signature of premixed ammonia-methane-air flames. *Combust. Flame* **2021**, *231*, 111508.
(30) Pugh, D.; Runyon, J.; Bowen, P.; Giles, A.; Valera-Medina, A.; Marsh, R.; Goktepe, B.; Hewlett, S. An investigation of ammonia primary flame combustor concepts for emissions reduction with OH*, NH_2* and NH* chemiluminescence at elevated conditions. *P Combust. Inst.* **2021**, *38*, 6451−6459.
(31) Mashruk, S.; Xiao, H.; Valera-Medina, A. Rich-Quench-Lean model comparison for the clean use of humidified ammonia/hydrogen combustion systems. *Int. J. Hydrogen Energy* **2021**, *46*, 4472−4484.
(32) Okafor, E. C.; Somarathne, K. D. K. A.; Hayakawa, A.; Kudo, T.; Kurata, O.; Iki, N.; Kobayashi, H. Towards the development of an efficient low-NO_x ammonia combustor for a micro gas turbine. *P Combust. Inst.* **2019**, *37*, 4597−4606.
(33) Li, S.; Zhang, S.; Zhou, H.; Ren, Z. Analysis of air-staged combustion of NH_3/CH_4 mixture with low NOx emission at gas turbine conditions in model combustors. *Fuel* **2019**, *237*, 50−59.
(34) Pugh, D.; Bowen, P.; Valera-Medina, A.; Giles, A.; Runyon, J.; Marsh, R. Influence of steam addition and elevated ambient conditions on NO_x reduction in a staged premixed swirling NH_3/H_2 flame. *P Combust. Inst.* **2019**, *37*, 5401−5409.
(35) Shrestha, K. P.; Lhuillier, C.; Barbosa, A. A.; Brequigny, P.; Contino, F.; Mounaïm-Rousselle, C.; Seidel, L.; Mauss, F. An experimental and modeling study of ammonia with enriched oxygen content and ammonia/hydrogen laminar flame speed at elevated pressure and temperature. *P Combust. Inst.* **2021**, *32*, 2163−2174.
(36) Ishihara, S.; Zhang, J.; Ito, T. Numerical calculation with detailed chemistry of effect of ammonia co-firing on NO emissions in a coal-fired boiler. *Fuel* **2020**, *266*, 116924.
(37) Shi, B.; Shimokuri, D.; Ishizuka, S. Reexamination on methane/oxygen combustion in a rapidly mixed type tubular flame burner. *Combust. Flame* **2014**, *161*, 1310−1325.
(38) Li, B.; Shi, B.; Zhao, X.; Ma, K.; Xie, D.; Zhao, D.; Li, J. Oxy-fuel combustion of methane in a swirl tubular flame burner under various oxygen contents: Operation limits and combustion instability. *Exp. Therm. Fluid Sci.* **2018**, *90*, 115−124.
(39) Wei, J.; Ren, Y.; Zhang, Y.; Shi, B.; Li, S. Effects of temperature-time history on the flame synthesis of nanoparticles in a swirl-stabilized tubular burner with two feeding modes. *J. Aerosol Sci.* **2019**, *133*, 72−82.
(40) Xu, Y.; Axt, C.; Song, M.; Kneer, R.; Li, S. Investigation on ignition behaviors of pulverized coal particles in a tubular swirl burner. *P Combust. Inst.* **2021**, *38*, 4179−4188.
(41) Shi, B.; Shimokuri, D.; Ishizuka, S. Methane/oxygen combustion in a rapidly mixed type tubular flame burner. *P Combust. Inst.* **2013**, *34*, 3369−3377.
(42) Hindasageri, V.; Vedula, R. P.; Prabhu, S. V. Thermocouple error correction for measuring the flame temperature with determination of emissivity and heat transfer coefficient. *Rev Sci Instrum.* **2013**, *84*, No. 024902.
(43) Nozari, H.; Karabeyoğlu, A. Numerical study of combustion characteristics of ammonia as a renewable fuel and establishment of reduced reaction mechanisms. *Fuel* **2015**, *159*, 223−233.

(44) *CHEMKIN-PRO 18.2*. San Diego: ANSYS, Inc.; 2017.
(45) Okafor, E. C.; Naito, Y.; Colson, S.; Ichikawa, A.; Kudo, T.; Hayakawa, A.; Kobayashi, H. Experimental and numerical study of the laminar burning velocity of CH_4−NH_3−air premixed flames. *Combust. Flame* **2018**, *187*, 185−198.
(46) Ishizuka, S.; Motodamari, T.; Shimokuri, D. Rapidly mixed combustion in a tubular flame burner. *P Combust. Inst.* **2007**, *31*, 1085−1092.
(47) Hayakawa, A.; Goto, T.; Mimoto, R.; Arakawa, Y.; Kudo, T.; Kobayashi, H. Laminar burning velocity and Markstein length of ammonia/air premixed flames at various pressures. *Fuel* **2015**, *159*, 98−106.
(48) Choe, J.; Sun, W.; Ombrello, T.; Carter, C. Plasma assisted ammonia combustion: Simultaneous NOx reduction and flame enhancement. *Combust. Flame* **2021**, *228*, 430−432.
(49) Hayakawa, A.; Arakawa, Y.; Mimoto, R.; Somarathne, K. D. K. A.; Kudo, T.; Kobayashi, H. Experimental investigation of stabilization and emission characteristics of ammonia/air premixed flames in a swirl combustor. *Int. J. Hydrogen Energy* **2017**, *42*, 14010−14018.
(50) Kurata, O.; Iki, N.; Inoue, T.; Matsunuma, T.; Tsujimura, T.; Furutani, H.; Kawano, M.; Arai, K.; Okafor, E. C.; Hayakawa, A.; Kobayashi, H. Development of a wide range-operable, rich-lean low-NO_x combustor for NH_3 fuel gas-turbine power generation. *P Combust. Inst.* **2019**, *37*, 4587−4595.
(51) Benés, M.; Pozo, G.; Abián, M.; Millera, Á.; Bilbao, R.; Alzueta, M. U. Experimental Study of the Pyrolysis of NH3 under Flow Reactor Conditions. *Energy Fuels* **2021**, *35*, 7193−7200.
(52) Hussein, N. A.; Agustin, V. M.; Alsaegh, A. S. Ammonia-hydrogen combustion in a swirl burner with reduction of NO_x emissions. *Energy Procedia* **2019**, *158*, 2305−2310.

https://doi.org/10.1021/acs.energyfuels.1c04004
Energy Fuels 2022, 36, 2277−2287